Kuramoto model for populations of quadratic integrate-and-fire neurons with chemical and electrical coupling

Cite as: Chaos **32**, 013105 (2022); https://doi.org/10.1063/5.0075285
Submitted: 14 October 2021 • Accepted: 13 December 2021 • Published Online: 03 January 2022

Pau Clusella, Bastian Pietras and Ernest Montbrió

Kuramoto model for populations of quadratic integrate-and-fire neurons with chemical and electrical coupling

Cite as: Chaos 32, 013105 (2022); doi: 10.1063/5.0075285
Submitted: 14 October 2021 · Accepted: 13 December 2021 ·
Published Online: 3 January 2022

Pau Clusella,[1,a)] Bastian Pietras,[2,3] and Ernest Montbrió[4]

AFFILIATIONS

[1]Department of Experimental and Health Sciences, Universitat Pompeu Fabra, Barcelona Biomedical Research Park, 08003 Barcelona, Spain
[2]Institute of Mathematics, Technical University Berlin, 10623 Berlin, Germany
[3]Bernstein Center for Computational Neuroscience Berlin, 10115 Berlin, Germany
[4]Neuronal Dynamics Group, Department of Information and Communication Technologies, Universitat Pompeu Fabra, 08018 Barcelona, Spain

Note: This article is part of the Focus Issue, Dynamics of Oscillator Populations.
[a)]**Author to whom correspondence should be addressed:** pau.clusella@upf.edu

ABSTRACT

We derive the Kuramoto model (KM) corresponding to a population of weakly coupled, nearly identical quadratic integrate-and-fire (QIF) neurons with both electrical and chemical coupling. The ratio of chemical to electrical coupling determines the phase lag of the characteristic sine coupling function of the KM and critically determines the synchronization properties of the network. We apply our results to uncover the presence of chimera states in two coupled populations of identical QIF neurons. We find that the presence of both electrical and chemical coupling is a necessary condition for chimera states to exist. Finally, we numerically demonstrate that chimera states gradually disappear as coupling strengths cease to be weak.

The Kuramoto model (KM) is a minimal mathematical model for investigating the emergence of collective oscillations in populations of heterogeneous, self-sustained oscillators.[1,2] Though the KM model was not originally intended to describe any specific natural system, an abundant body of work applies it to explore large-scale neuronal oscillations; see, e.g., Refs. 3–22. Yet, it remains unclear how the parameters of the KM relate to parameters—such as chemical or electrical synaptic strengths—critical for setting up synchronization in biophysically realistic neuronal models.[23,24] Here, we unveil a mathematical relation between a popular spiking neuron model, the quadratic integrate-and-fire (QIF),[25–27] with a well-known variant of the KM.[28,29] This provides support in favor of the use of the KM for modeling studies in computational neuroscience and introduces the powerful mathematical framework of the KM[30–32] for the analysis of the dynamics of QIF networks.

I. INTRODUCTION

Large-scale neuronal oscillations emerge due to the synchronous interplay of ensembles of neurons. These oscillations are successfully replicated by mathematical models of spiking neurons, which also allow for a mechanistic understanding of neuronal rhythmogenesis.[23,24] According to these theories, inhibitory synapses play a central role in setting up neuronal synchronization either in isolation[33] or due to their interplay with excitatory neurons.[34] Additionally, inhibitory cells are very often coupled electrically, and this coupling is usually mediated by so-called gap junctions.[35] Such electrical synapses are well-known to largely favor synchrony.

Recently, important efforts have been put forward to model the oscillatory dynamics of so-called whole-brain networks.[3,4,36] To facilitate both the analysis and the computational work, many studies do not use spiking neuron models but apply the mathematical framework of the Kuramoto model (KM); see, e.g., Refs. 3–22.

Yet, it remains unclear how to relate the parameters of the KM to bio-physically meaningful parameters, such as synaptic strengths.

In this paper, we aim to theoretically substantiate the use of the KM for neuronal modeling by providing a mathematical link between the quadratic integrate-and-fire (QIF) model and the KM. We derive a KM for QIF neurons and subsequently justify its validity in two different ways: First, we compare the predictions of the KM with those of an exact mean-field model for QIF neurons—often referred to as firing rate or neural mass model (NMM).[37–39] Second, we use two populations of *identical* Kuramoto oscillators to find so-called chimera states.[40–43] In a chimera state, one of the two homogeneous populations displays in-phase synchrony, and NMMs are useless in this case. However, the KM for QIF neurons is perfectly suited to describe full synchrony, and we exploit this to uncover the existence of chimera states in two-population networks of QIF neurons.

Our derivation of the KM for QIF neurons mainly builds on a previous work by Izhikevich[27] and also on Refs. 44 and 45. In Chap. 10 of Ref. 27, Izhikevich applied perturbation methods to derive a simplified model that approximated the dynamics of two identical QIF neurons with *either* chemical or electrical coupling.[46] Here, we extend the work of Izhikevich and derive a model that approximates the dynamics of an *ensemble of heterogeneous* QIF neurons with *both* chemical and electrical coupling. The approximated model turns out to be a well-known version of the KM[28,29] and is valid when both heterogeneities and coupling strengths are weak.

This paper is organized as follows: In Sec. II, we introduce the QIF population model, and in Sec. III, we describe the method to reduce the QIF model to the KM. In Sec. IV, we analyze the dynamics of the KM and demonstrate that it correctly describes the collective dynamics of populations of nearly identical QIF neurons, with weak electrical and chemical synapses. In Sec. V, we exploit the KM to uncover the presence of chimera states in coupled populations of identical QIF neurons. Finally, in Sec. VI, we briefly discuss and summarize our results.

II. POPULATION OF QIF NEURONS WITH ELECTRICAL AND CHEMICAL SYNAPSES

We investigate a population of N quadratic integrate-and-fire (QIF) neurons $i = 1, \ldots, N$ interacting all-to-all via both electrical and chemical synapses,[37,47,48,90]

$$\tau \dot{V}_i = V_i^2 + \eta_i + \varepsilon\, I_{i,syn}(t) \text{ if } V_i > V_p, \text{ then } V_i \leftarrow V_r, \tag{1}$$

where V_i is the membrane potential of neuron i, τ is the membrane time constant of the neurons, and η_i represents an external current, which varies from cell to cell. Due to the quadratic nonlinearity of the QIF model, the membrane potential blows up in finite time, and a resetting rule is needed: When the neurons reach the peak value V_p, they emit a spike and the voltage is reset to V_r. We assume symmetric spike resetting, $V_p = -V_r$ and $V_p \to \infty$, so that the QIF model is equivalent to the so-called theta-neuron.[25,26] In addition, we consider $\eta_i > 0$, and hence, in the absence of synaptic inputs ($I_{i,syn} = 0$), QIF neurons are self-sustained oscillators. Finally, synaptic inputs (whose total strength is controlled by the *small* parameter $\varepsilon \geq 0$) are composed of electrical and chemical synapses,

$$I_{i,syn}(t) = g(v(t) - V_i) + J\tau r(t). \tag{2}$$

Specifically, electrical synapses (of strength $\varepsilon g \geq 0$) diffusively couple each neuron with the mean membrane potential,

$$v(t) = \frac{1}{N}\sum_{j=1}^{N} V_j(t). \tag{3}$$

Electrical synapses mostly connect inhibitory neurons, and hence, the chemical synaptic strength, J, is thought of as a negative parameter thereafter. Finally, chemical synapses (of strength εJ) are mediated by the mean firing rate,

$$r(t) = \frac{1}{N}\sum_{j=1}^{N}\sum_{k}\delta\left(t - t_j^{(k)}\right), \tag{4}$$

where $t_j^{(k)}$ is the time of the kth spike of the jth neuron and $\delta(t)$ is the Dirac delta function.

III. DERIVATION OF THE KURAMOTO MODEL FOR POPULATIONS OF QIF NEURONS

In the following, we derive the Kuramoto model corresponding to Eq. (1). The derivation exploits well-known mathematical methods that are reviewed, for example, in Refs. 27, 49, and 50.

We perform the derivation of the KM as follows: First, we obtain the phase resetting curve (PRC) of the QIF model. Second, invoking weak coupling, we derive the so-called Winfree model corresponding to the QIF model. Finally, we assume weak heterogeneity and apply the method of averaging to obtain the Kuramoto model corresponding to Eq. (1).

A. Phase resetting curve (PRC) of a QIF neuron

We first consider an isolated, regularly spiking QIF neuron; i.e., $I_{i,syn} = 0$ and $\eta_i > 0$. The solution of the QIF model immediately after a spike, $V_i(0) = -\infty$, is

$$V_i(t) = \sqrt{\eta_i}\tan\left(t\sqrt{\eta_i}/\tau - \pi/2\right). \tag{5}$$

The frequency of the oscillations is

$$\Omega_i = 2\sqrt{\eta_i}/\tau, \tag{6}$$

and a phase variable θ_i can be defined in the interval $[0, 2\pi)$ as

$$\theta_i = \Omega_i t = 2\arctan(V_i/\sqrt{\eta_i}) + \pi. \tag{7}$$

Next, we assume that the neuron is perturbed so that its membrane potential instantaneously changes from V_i to $V_i + \delta V$. Then, the new phase after the perturbation is $\theta_{i,new} = 2\arctan((V_i + \delta V)/\sqrt{\eta_i}) + \pi$.

The PRC measures the phase shift produced by the perturbation; i.e., PRC $= \theta_{i,new} - \theta_i$. Hence, for the QIF model, the PRC is[27]

$$\mathrm{PRC}(\theta_i, \delta V) = 2\arctan(\delta V/\sqrt{\eta_i} - \cot(\theta_i/2)) + \pi - \theta_i. \tag{8}$$

This function depends on both the strength of the perturbation and the phase of the neuron at the instant of the perturbation. The PRC

[Eq. (8)] is always positive, indicating that positive/negative perturbations only produce positive/negative phase shifts. This characterizes the so-called Class 1 neuronal oscillators.[25]

B. Weak coupling approximation and the Winfree model

The PRC [Eq. (8)] exactly characterizes the phase response of the QIF neuron to a perturbation. Next, we invoke weak coupling, which allows for deriving a new phase model—called the Winfree model—that approximates the network [Eq. (1)] for $\varepsilon \ll 1$.

Weak perturbations produce small changes in the membrane potential, $|\delta V| \ll 1$. Then, the PRC scales linearly with the strength of the perturbation,[51]

$$\mathrm{PRC}(\theta_i, \delta V) \approx Z(\theta_i)\delta V,$$

where $Z(\theta_i)$ is called phase sensitivity function or infinitesimal phase resetting curve (iPRC). For the QIF model, the iPRC is

$$Z(\theta_i) = \left.\frac{\partial \mathrm{PRC}(\theta_i, \delta V)}{\partial(\delta V)}\right|_{\delta V=0} = \frac{1-\cos\theta_i}{\sqrt{\eta_i}}. \tag{9}$$

When weak perturbations are described by a continuous function $P(t)$ with $|P(t)| \ll 1$, the infinitesimal change in the phase due to the perturbations is $d\theta = Z(\theta)P(t)dt$. Accordingly, assuming weak coupling $\varepsilon \ll 1$, the population of QIF neurons [Eq. (1)] is well approximated by the Winfree model,

$$\dot{\theta}_i = \Omega_i + \frac{\varepsilon}{\tau}(1-\cos\theta_i)\sum_{j=1}^{N} P(\theta_i, \theta_j), \tag{10}$$

where perturbations to neuron i are due to synaptic inputs from neuron j and can be written in terms of the phase variables as

$$P(\theta_i, \theta_j) = \frac{g}{N}\left(\cot(\theta_i/2) - \sqrt{\frac{\eta_j}{\eta_i}}\cot(\theta_j/2)\right) + \frac{2J}{N}\sqrt{\frac{\eta_j}{\eta_i}}\delta(\theta_j). \tag{11}$$

Recall that $\theta_j \in [0, 2\pi)$ so that the Dirac delta function in Eq. (11) has argument zero whenever neuron j fires a spike.

C. Weak heterogeneity and the averaging approximation

The Winfree model can be further simplified using the method of averaging. We consider the external currents in Eq. (1) as a common current $\bar{\eta}$ plus a weakly distributed parameter as

$$\eta_i = \bar{\eta} + \varepsilon\chi_i. \tag{12}$$

In the derivation of the Winfree model, we already assumed weak coupling, $\varepsilon \ll 1$. Therefore, the smallness of parameter ε implies now the smallness of both coupling terms and the level of heterogeneity. This assumption allows for a separation of time scales so that the phases θ_i can be written as

$$\theta_i = \Phi + \phi_i, \tag{13}$$

where Φ describes the fast, free-running oscillation of period

$$T = \tau\pi/\sqrt{\bar{\eta}},$$

whereas the phases ϕ_i describe slow phase drifts produced by weak heterogeneities and synaptic inputs. Substituting Eq. (13) into the Winfree model [Eqs. (10) and (11)] and collecting terms of order ε, we find the evolution equation for the slow phases,

$$\dot{\phi}_i = \frac{\varepsilon\chi_i}{\tau\sqrt{\bar{\eta}}} + [1-\cos(\Phi+\phi_i)]\frac{\varepsilon}{\tau N}\sum_{j=1}^{N} p(\Phi+\phi_i, \Phi+\phi_i+\Delta_{ji}). \tag{14}$$

Here, we defined pairwise phase differences as $\Delta_{ji} = \phi_j - \phi_i$ and a function describing synaptic perturbations as

$$p(x,y) = g\left[\cot(x/2) - \cot(y/2)\right] + 2J\delta(y).$$

To apply the method of averaging to Eq. (14), we consider that in one period of the fast oscillation, T, the slow phases ϕ_i can be assumed constant. Then, Eq. (14) reduces to

$$\dot{\phi}_i = \frac{\varepsilon}{\tau N}\sum_{j=1}^{N}\Gamma(\Delta_{ji}), \tag{15}$$

where the coupling function Γ is obtained by averaging the r.h.s. of Eq. (14) over one period T. This involves the evaluation of four integrals that can be explicitly computed and yields the phase interaction function

$$\Gamma(\Delta_{ji}) = \frac{\chi_i}{\sqrt{\bar{\eta}}} + g\sin\Delta_{ji} + \frac{J}{\pi}(1-\cos\Delta_{ji}). \tag{16}$$

D. Kuramoto model for populations of QIF neurons

Substituting Eq. (16) into Eq. (15) and expressing the result in terms of the original phases [Eq. (13)], we find the Kuramoto model

$$\dot{\theta}_i = \omega_i + \frac{\varepsilon}{\tau N}\sum_{j=1}^{N}\left[g\sin(\theta_j-\theta_i) - \frac{J}{\pi}\cos(\theta_j-\theta_i)\right] + \frac{\varepsilon}{\tau}\frac{J}{\pi}, \tag{17}$$

with natural frequencies

$$\omega_i = \frac{2\sqrt{\bar{\eta}}}{\tau} + \varepsilon\frac{\chi_i}{\tau\sqrt{\bar{\eta}}}. \tag{18}$$

In the absence of electrical synapses $g = 0$, Eq. (17) essentially[52] reduces to the Kuramoto model with chemical synapses derived in Refs. 44 and 45. The KM for QIF neurons [Eq. (17)] generalizes the results in Refs. 44 and 45 to networks with both electrical and chemical coupling, and it is our main result.

Equation (18) is the linear approximation of Eq. (6) for weak heterogeneity—see also Eq. (12). The last term of Eq. (17) describes the deviation of the natural frequencies due to synaptic coupling, which exclusively depends on chemical coupling. Excitatory coupling ($J > 0$) speeds up the frequencies of the oscillators, and inhibition ($J < 0$) slows them down. These frequency shifts do not qualitatively affect the collective dynamics of Eq. (17), but they may become relevant if the oscillators are not all-to-all coupled[28,53] or in the case of interacting excitatory and inhibitory populations.[45]

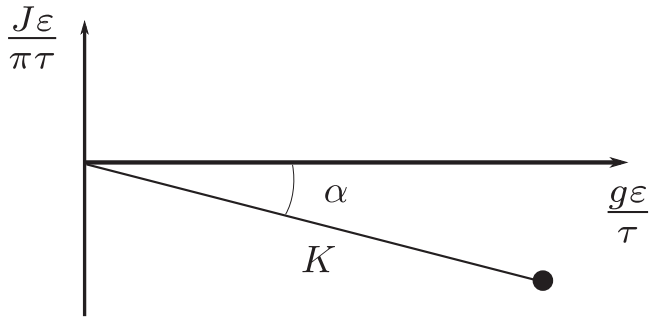

FIG. 1. Geometric relation—determined by Eqs. (20) and (21)—between the coupling parameters of the QIF model [Eq. (1)] and the Kuramoto model [Eq. (19)].

Alternatively, Eq. (17) can be cast in the more transparent form,[28,29]

$$\dot{\theta}_i = \omega_i + \frac{K}{N}\sum_{j=1}^{N}\left[\sin(\theta_j - \theta_i - \alpha) + \sin\alpha\right], \tag{19}$$

with the coupling constant

$$K = \frac{\varepsilon}{\tau}\sqrt{(J/\pi)^2 + g^2} \tag{20}$$

and the phase lag parameter

$$\alpha = \arctan\left(\frac{J/\pi}{g}\right). \tag{21}$$

The coupling parameters K and α satisfy a simple geometric relation with the coupling parameters of the QIF model [Eq. (1)], illustrated in Fig. 1. Given a particular choice of the QIF coupling parameters, Fig. 1 shows that electrical coupling and chemical coupling (divided by a factor π) contribute equally to the overall coupling strength K of the KM and that K is insensitive to the sign of the chemical coupling—in Fig. 1, we consider an inhibitory network; i.e., $J < 0$.

To lighten the notation, we consider $\varepsilon = 1$ thereafter. Hence, for the KM [Eq. (19)] to be a good approximation of Eq. (1), in the following, the synaptic weights J and g need to be regarded as small quantities.

IV. ANALYSIS OF THE KURAMOTO MODEL FOR QUADRATIC INTEGRATE-AND-FIRE NEURONS

Using Fig. 1—or, equivalently, Eq. (21)—we may infer how chemical and electrical synapses contribute to synchronization, using well-known results for the KM. For example, the phase constant α critically determines the synchronization behavior of Eq. (19).[29] In the absence of electrical coupling, $g = 0$, we find $\alpha = +\pi/2$ for excitatory coupling and $\alpha = -\pi/2$ for inhibitory coupling. This indicates that collective synchronization is unreachable—consistent with the well-known fact that instantaneous chemical coupling is unable to synchronize type 1 neuronal oscillators.[25,54,55] In contrast, in the absence of chemical coupling, one finds $\alpha = 0$, and Eq. (19) reduces to the standard KM, in which collective synchronization is achieved at a critical degree of heterogeneity $\Delta = \Delta_c(K)$ that depends on the coupling strength.[2] Between these two extreme cases, that is, in networks with both electrical and chemical synapses, we find the phase lag parameter $|\alpha| \in (0, \pi/2)$, and synchronization generally depends on both α and the overall shape of the distribution of natural frequencies.[29]

To validate the KM for QIF neurons, in Sec. IV A, we obtain the mean-field model corresponding to Eq. (19) and compare its predictions with those of the mean-field model derived in Ref. 37, which describes the dynamics of the QIF network [Eq. (1)] exactly.

A. Mean-field model

In the thermodynamic limit ($N \to \infty$), the dynamics of Eq. (19) are greatly simplified assuming χ_i in Eq. (18) to be Lorentzian-distributed,

$$G(\chi) = \frac{\Delta/\pi}{\chi^2 + \Delta^2},$$

where Δ is the half-width of the distribution. Then, using the so-called Ott–Antonsen (OA) ansatz,[56] the KM [Eq. (19)] can be exactly reduced to a mean-field model consisting of two differential equations for the complex Kuramoto order parameter,

$$Z = Re^{i\psi} = \frac{1}{N}\sum_{j=1}^{N} e^{i\theta_j} \tag{22}$$

in the limit $N \to \infty$. The mathematical approach to obtain the mean-field equations corresponding to Eq. (19) is a standard procedure. Here, we skip the mathematical details and refer the reader to, for example, Ref. 57, where the mean-field model corresponding to Eq. (19) was derived in detail. Accordingly, using Eqs. (18), (20), and (21), we obtain the mean-field equations

$$\dot{R} = \frac{R}{2\tau}\left(-\frac{2\Delta}{\sqrt{\bar{\eta}}} + g(1 - R^2)\right), \tag{23a}$$

$$\dot{\psi} = \frac{2\sqrt{\bar{\eta}}}{\tau} + \frac{J}{2\pi\tau}(1 - R^2), \tag{23b}$$

which approximate the dynamics of the QIF model [Eq. (1)] for small g and J. The radial equation Eq. (23a) shows that the incoherent state ($R = 0$) is a stable fixed point above the critical width,

$$\Delta_c = g\sqrt{\bar{\eta}}/2, \tag{24}$$

which is independent of chemical coupling, J. At $\Delta = \Delta_c$, a stable nontrivial solution—corresponding to a partially synchronized state—bifurcates from incoherence with amplitude

$$R = \sqrt{(\Delta_c - \Delta)/\Delta_c}$$

and frequency

$$\Omega = \frac{2\sqrt{\bar{\eta}}}{\tau} + \frac{\Delta}{\tau\pi\sqrt{\bar{\eta}}}\frac{J}{g}. \tag{25}$$

The solid line in Fig. 2 corresponds to the critical boundary [Eq. (24)], while dashed lines correspond to the exact synchronization boundaries of the QIF network for various degrees of inhibitory coupling—see Eq. (7) in Ref. 37. Note that for weak electrical coupling and/or weak heterogeneity, all boundaries approach Eq. (24).

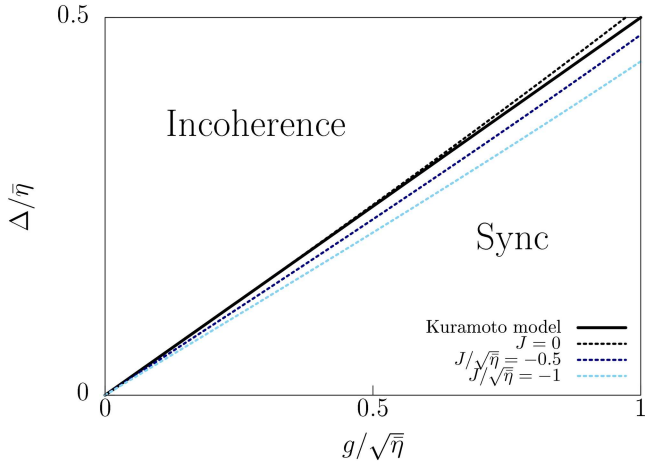

FIG. 2. Synchronization boundary of the QIF network [Eq. (1)] with the Lorentzian distribution of currents for various values of the (scaled) inhibitory coupling strength, $J/\sqrt{\bar{\eta}}$. The solid line corresponds to the approximated critical width [Eq. (24)], which is independent of J. Dashed lines correspond to the exact synchronization boundaries, obtained using Eq. (7) in Ref. 37.

Furthermore, for weak heterogeneity, the frequency of the synchronized cluster [Eq. (25)] agrees with Eq. (8) in Ref. 37, which describes the frequency of the oscillations near their onset.

In sum, these results confirm the validity of the Kuramoto model [Eq. (19)] as an approximation of a population of heterogeneous QIF neurons with electrical and chemical coupling [Eq. (1)].

V. CHIMERA STATES IN COUPLED HOMOGENEOUS POPULATIONS OF QIF NEURONS

To further illustrate the appropriateness of the KM to investigate the dynamics of QIF networks, we investigate the presence of chimera states in populations of QIF neurons. Our motivation is threefold:

1. Chimera states were originally uncovered in a nonlocally coupled network of identical Kuramoto oscillators.[58] Given that the phase dynamics [Eq. (19)] are an approximation of Eq. (1) valid for weak heterogeneity and weak coupling, we expect QIF networks to display similar chimera states, at least for weak coupling.
2. Several papers have been devoted to investigate chimera states in networks of spiking neurons; see, e.g., Refs. 59–69. Some of them provide numerical evidence that the presence of both chemical and electrical synapses favors the emergence of chimera states.[65,67] Yet, the relation between chimera states in spiking neuron networks with the original chimera states uncovered in the KM[40–42,58] is lacking.[70–72]
3. Recently, exact mean-field models for large populations of QIF neurons (often called neural mass models, NMMs) with electrical and chemical synapses have been put forward.[37,38,48,73] However, such NMMs have an important limitation when neurons are—as in a chimera state—identical and fully synchronized since both the mean membrane potential and the mean firing rate diverge at the instant of collective firing.[74] This divergence is avoided using the averaging approximation, and hence, the KM for QIF neurons, Eq. (17), becomes singularly suited to study collective behavior where neurons are fully synchronized.

Chimera states were originally uncovered in a ring of identical Kuramoto oscillators with nonlocal coupling when $\alpha \lesssim \pi/2$.[58] Shortly after their discovery, chimera states were also found in a simpler setup, consisting of two populations of identical Kuramoto oscillators.[40,41] Here, to investigate chimera states in networks of QIF neurons, we adopt the two-population setup of Refs. 40 and 41.

Specifically, we analyze the dynamics of two identical populations (labeled $\sigma \in \{1,2\}$) of $n = N/2$ identical QIF neurons, interacting all-to-all via both chemical and electrical synapses,

$$\tau \dot{V}_i^\sigma = \left(V_i^\sigma\right)^2 + \bar{\eta} + I_{i,syn,s}^\sigma + I_{i,syn,c}^\sigma, \tag{26}$$

with the resetting rule of Eq. (1). Synaptic inputs have a contribution $I_{i,syn,s}^\sigma$ due to self-interactions within each population σ and another contribution $I_{i,syn,c}^\sigma$ due to cross-interactions of population $\sigma = \{1,2\}$ with population $\sigma' = \{2,1\}$,

$$I_{i,syn,s}^\sigma = g_s(v^\sigma - V_i^\sigma) + J_s \tau r^\sigma,$$
$$I_{i,syn,c}^\sigma = g_c(v^{\sigma'} - V_i^\sigma) + J_c \tau r^{\sigma'}.$$

Here, v^σ and r^σ are the mean membrane voltage and the mean firing rate of population σ, respectively. Using Eqs. (19)–(21), it is straightforward to write the KM corresponding to Eq. (26) as

$$\dot{\theta}_i^\sigma = \omega + \frac{K_s}{n}\sum_{j=1}^{n}\left[\sin\left(\theta_j^\sigma - \theta_i^\sigma - \alpha_s\right) + \sin\alpha_s\right]$$
$$+ \frac{K_c}{n}\sum_{j=1}^{n}\left[\sin\left(\theta_j^{\sigma'} - \theta_i^\sigma - \alpha_c\right) + \sin\alpha_c\right], \tag{27}$$

with $\omega = 2\sqrt{\bar{\eta}}/\tau$ and

$$K_{s,c} = \frac{1}{\tau}\sqrt{(J_{s,c}/\pi)^2 + g_{s,c}^2}, \tag{28}$$

$$\alpha_{s,c} = \arctan\left(\frac{J_{s,c}/\pi}{g_{s,c}}\right). \tag{29}$$

The KM [Eq. (27)] is slightly more general than the model originally investigated in Refs. 40, 42—in which the authors considered $\alpha_c = \alpha_s$. In the QIF network, this equality of the phase lag parameters implies that the ratios of chemical to electrical coupling

$$\rho_s = \frac{J_s/\pi}{g_s}, \quad \rho_c = \frac{J_c/\pi}{g_c}, \tag{30}$$

are identical, $\rho_s = \rho_c$. Recent work has also considered the dynamics of chimera states in populations of Kuramoto oscillators with distributed phase lags.[43,75] Specifically, Martens *et al.*[43] investigated chimera states in the two-population model [Eq. (27)].

A. Mean-field model

As we discussed previously, in the thermodynamic limit ($n = N/2 \to \infty$), the KM can be exactly reduced to a low-dimensional mean-field model using the OA ansatz. In the case of the homogeneous, two-population Kuramoto model [Eq. (27)], the dynamics reduces to six ordinary differential equations using the Watanabe–Strogatz ansatz.[76,77,91] Assuming a particular set of initial conditions for the phases, the system further reduces to four differential equations and it is described by the OA ansatz.[41,76] Such mean-field equations describe the evolution of the complex Kuramoto order parameters of the two populations,

$$Z_\sigma = R_\sigma e^{i\psi_\sigma} = \frac{1}{n}\sum_{j=1}^{n} e^{i\theta_j^\sigma}. \tag{31}$$

Using the mean-field analysis in Refs. 43 and 78 and Eqs. (28)–(30), the mean-field equations for the complex Kuramoto order parameters can be further reduced (by virtue of the rotational symmetry of the KM) to the three dimensional system,

$$\frac{dR_1}{d\tilde{t}} = \frac{1-R_1^2}{2}\left[R_1 + \frac{g_c}{g_s}R_2\cos\Psi - \rho_s\frac{J_c}{J_s}R_2\sin\Psi\right], \tag{32a}$$

$$\frac{dR_2}{d\tilde{t}} = \frac{1-R_2^2}{2}\left[R_2 + \frac{g_c}{g_s}R_1\cos\Psi + \rho_s\frac{J_c}{J_s}R_1\sin\Psi\right], \tag{32b}$$

$$\frac{d\Psi}{d\tilde{t}} = \rho_s\frac{R_1^2-R_2^2}{2R_1R_2}\left(\frac{J_c}{J_s}\cos\Psi - R_1R_2\right) - \frac{g_c}{g_s}\frac{R_1^2+R_2^2+2R_1^2R_2^2}{2R_1R_2}\sin\Psi, \tag{32c}$$

where the phase difference between the complex order parameters [Eq. (31)] is defined as $\Psi = \psi_1 - \psi_2$. In addition, we have rescaled time as $\tilde{t} = g_s t/\tau$ so that the dynamics of Eq. (27) depends only on three combinations of parameters: the ratios of cross to self couplings g_c/g_s and J_c/J_s and the ratio of chemical to electrical coupling ρ_s—see Eq. (30). In contrast, the original QIF model [Eq. (26)] can, after appropriate rescaling, only be reduced to involve at least four parameters.

B. Phase diagram of the mean-field model

Chimera states in two-population Kuramoto networks correspond to symmetry-broken states where one of the populations is fully synchronized (i.e., $R_\sigma = 1$), while the other remains only partially synchronized ($R_{\sigma'} < 1$). In addition, chimera states in two-population networks of identical Kuramoto oscillators coexist with the fully synchronized state, $R_1 = R_2 = 1$.[40–42]

To obtain the phase diagrams depicted in Fig. 3, we set $R_2 = 1$ in Eq. (32) and numerically continued[79] chimera states using initial conditions in their basin of attraction—see Fig. 4(a) and Ref. 41. The diagrams show the regions where steady (shaded) and unsteady (hatched) chimera states are stable for two different values of the ratio ρ_s; see Eq. (30). These regions lie between saddle-node (red) and homoclinic (green) bifurcation lines, which—together with a Hopf (blue) bifurcation line separating steady and unsteady chimera states—meet at two Takens–Bogdanov (TB) points. For decreasing $|\rho_s|$, the region of chimera states shrinks and eventually disappears when the two TB points collide.

The phase diagrams in Fig. 3 are qualitatively identical to that of Fig. 4(a) in Ref. 43, but here, the regions of chimeras are represented in the parameter space of the QIF model.[80] This allows us to

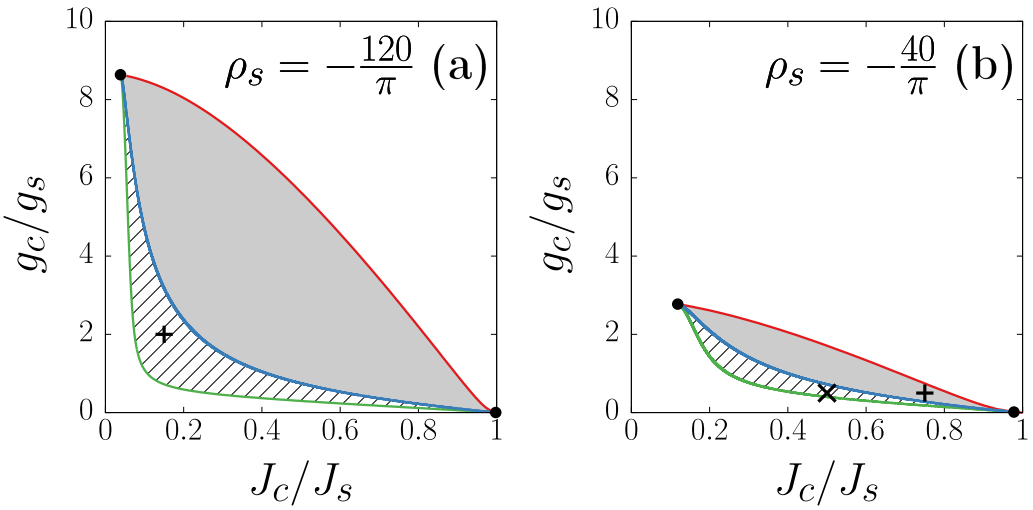

FIG. 3. Phase diagrams of the mean-field model [Eq. (32)] for two values of the ratio ρ_s; see Eq. (30). Shaded and hatched regions correspond to regions of steady and unsteady stable chimera states, respectively. Red lines: Saddle-node (SN) bifurcations. Blue lines: Hopf bifurcations. Green lines: Homoclinic bifurcations. Filled circles: Takens–Bogdanov points. In panel (a), the + symbol corresponds to the coordinates used for the numerical simulations of the QIF network depicted in Figs. 4(f)–4(h): $J_c/J_s = 0.15$, $g_c/g_s = 2.0$. In panel (b), symbols correspond to the coordinates used for the numerical simulations of the QIF network depicted in Figs. 4(b)–4(d) and Fig. 5: $J_c/J_s = 0.75$, $g_c/g_s = 0.5$ (+ symbol) and in Fig. 6: $J_c/J_s = 0.5$, $g_c/g_s = 0.5$ (× symbol).

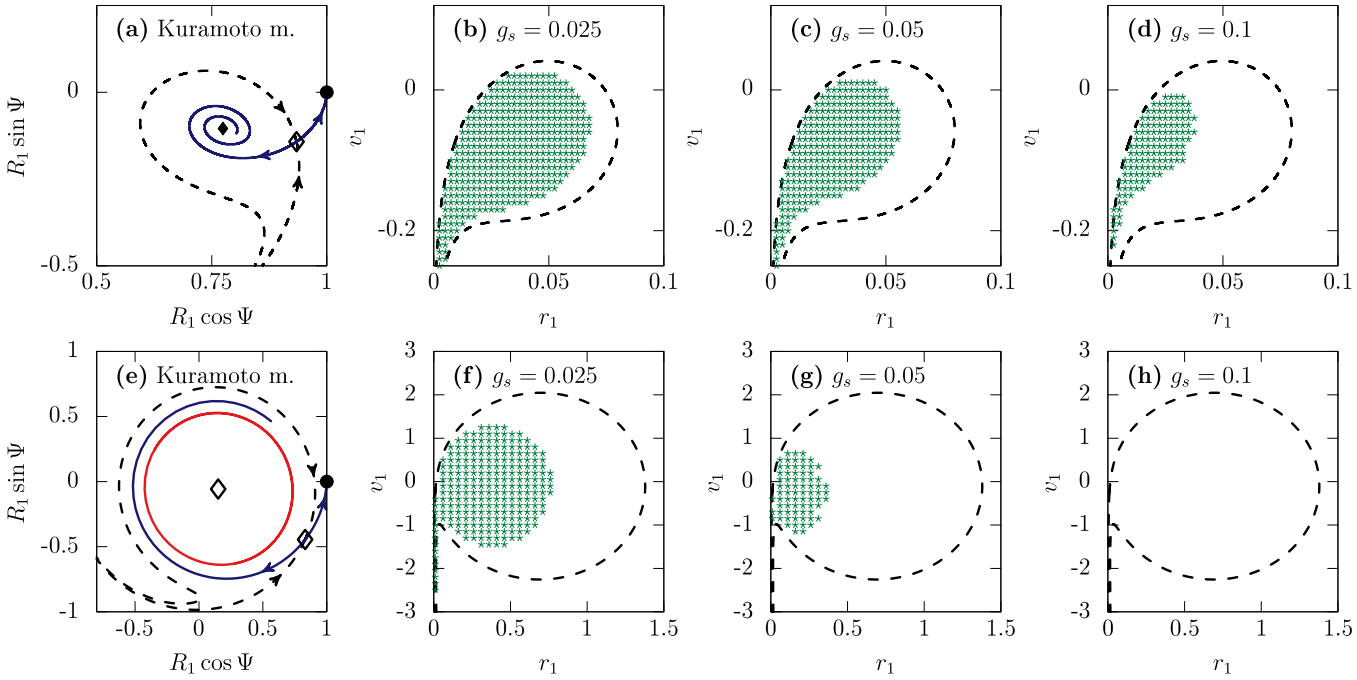

FIG. 4. Basins of attraction of chimera states in the two-population KM (dashed lines) and in the two-population QIF model (green-dotted regions). Panels (a)–(d): Phase portraits of the (a) KM and (b)–(d) QIF model, with $J_c/J_s = 0.75$, $g_c/g_s = 0.5$, $\rho_s = -40/\pi$; see $\times$ symbol in Fig. 3(b). Panels (e)–(h): Phase portraits of the (e) KM and (f)–(h) QIF model, with $J_c/J_s = 0.15$, $g_c/g_s = 2$, $\rho_s = -120/\pi$; see $+$ symbol in Fig. 3(a). Symbols and lines in panels (a) and (e): Solid/open diamond: Stable/unstable chimera states, respectively; solid dot: In-phase synchronized state. Solid blue line: Unstable manifold of the saddle point. Dashed black lines: Stable manifold of the saddle point, basin of attraction of stable chimeras. The basins of attraction of chimeras have been transformed from the $(R_1 \cos \Psi, R_1 \sin \Psi)$ coordinates [panels (a) and (e)] to the (r_1, v_1) coordinates [panels (b)–(d) and (f)–(h)] using Eq. (33). Green dots correspond to initial values leading to chimera states after $t = 2500$ time units in numerical simulations of two populations of $n = 200$ QIF neurons. Parameters: $\tau = 1$ and $\eta = 1$. Simulations using the Euler scheme with time step: $dt = 10^{-4}$ and symmetric resetting: $V_p = -V_r = 1000$.

determine three necessary conditions for the existence of chimera states in two-population networks of QIF neurons:

1. Chimera states only exist in the presence of *both* chemical and electrical coupling.
2. Self-chemical coupling needs to be much larger than self-electrical coupling, $|J_s| \gg g_s$ —or, equivalently, $|\rho_s| \gg 1$. Using Eq. (29), this implies that α_s is close to $\pm\pi/2$ in correspondence with the previous work.[40,41,43]
3. The modulus of self-chemical coupling needs to be larger than that of cross-chemical coupling, $|J_s| > |J_c|$.

These three conditions are not sufficient conditions to have chimera states in Eq. (26) though. Indeed, Eq. (27) and the corresponding mean field [Eq. (32)] are an approximation of the full QIF network [Eq. (26)] for weak coupling, but it remains to be seen whether chimera states persist in QIF networks when coupling strengths become stronger. We numerically explore this issue in Sec. V C.

C. Chimera states in populations of QIF neurons

In the following, we numerically investigate the presence of chimera states in the spiking neuron network model of QIF neurons [Eq. (26)]. First, we confirm that, for weak coupling, chimeras are present in QIF networks, and they exist in the parameter range predicted by the phase diagrams of the KM (Fig. 3). However, then, we show that the basin of attraction of chimera states shrinks as synaptic coupling strengths become stronger.

1. Dynamics of chimera states

Using the OA ansatz, the dynamics of the two-population model [Eq. (27)] with $N \to \infty$ can be exactly reduced to the three-dimensional system [Eq. (32)]. In a chimera state, we may set $R_2 = 1$ so that Eq. (32) further reduces to a planar system with variables R_1 and Ψ. Figures 4(a) and 4(e) show the basins of attraction (dashed lines) of (a) a steady chimera state (solid diamond symbol) and of (e) an unsteady chimera state (red limit cycle), with parameters corresponding to $+$ symbols in Fig. 3. As mentioned previously, chimera states coexist with the stable fully synchronized solution (solid dot symbols), $Z_1 = R_1 = 1$, $\Psi = 0$. The basin of attraction of the chimera state is defined by the stable manifold of a saddle point (open diamond symbols).[41]

To set initial conditions leading to the chimera state of Fig. 4(a) in the network of QIF neurons, we considered the initial condition $Z_2 = 1$ and $Z_1 = R_1 e^{i\Psi}$—with R_1 and Ψ such that the system is in

the basin of attraction of the steady chimera state. Then, we used the conformal map,[39]

$$\pi r_\sigma - i v_\sigma = \frac{1 - Z_\sigma}{1 + Z_\sigma}, \tag{33}$$

to transform the mean-field coordinates Z_2 and Z_1 into the mean firing rate r and the mean membrane potential v of the populations of QIF neurons—for population 2, we find $\pi r_2 + i v_2 = 0$. Then, we initialized the membrane voltages of the populations according to the formula $V_i(0) = v + (\pi\tau r)\tan[\pi/2(2i - n - 1)/(n + 1)]$ for $i = 1, \ldots, n$.[81]

In Fig. 5, we show the results of a numerical simulation of the QIF network ($g_s = 0.1$). The raster plot in Fig. 5(a) clearly shows the signature of a chimera state: Neurons in population 1 (blue) are only partially synchronized, while neurons in population 2 remain fully synchronized. The time evolution of the firing rate r_1 and the mean membrane potential v_1 for the incoherent group are displayed in Figs. 5(b) and 5(c), respectively. These collective variables indicate a periodic evolution of the incoherent population, with fluctuations caused by the finite resetting of the QIF neurons and by finite-size effects. Finally, Fig. 5(d) shows the Kuramoto order parameter R_1 (blue) obtained using the time series $r_1(t)$ and $v_1(t)$ and the conformal map [Eq. (33)]. In contrast with the steady chimera state in the mean field [Eq. (32)] (black dotted line), the chimera state in the network of QIF neurons is not stationary but oscillates periodically in time. The same unsteady chimeras arise in two-population networks of Winfree oscillators[44] and are the consequence of the lack of rotational symmetry in the Winfree and QIF models.

In Fig. 6, we also explored how the unsteady chimera states in the Kuramoto model [Eq. (27)] translate to networks of QIF neurons. To this aim, we set the parameters of the QIF model in the hatched region of the bifurcation diagram in Fig. 3(b) (× symbol) and used the same initial conditions as in the previous simulation. Here, we find a more complex chimera state that seems to display macroscopic quasiperiodic dynamics:[82] both the firing rate and the mean membrane potential of the incoherent population oscillate with two characteristic frequencies as can be appreciated in Figs. 6(b) and 6(c). Again, the quasiperiodic chimera state in the QIF network corresponds to a periodic chimera state in the Kuramoto model. In Fig. 5(d), we used Eq. (33) to represent the Kuramoto order parameter for the QIF network (blue), which roughly approximates the periodic dynamics of the corresponding equation (32).

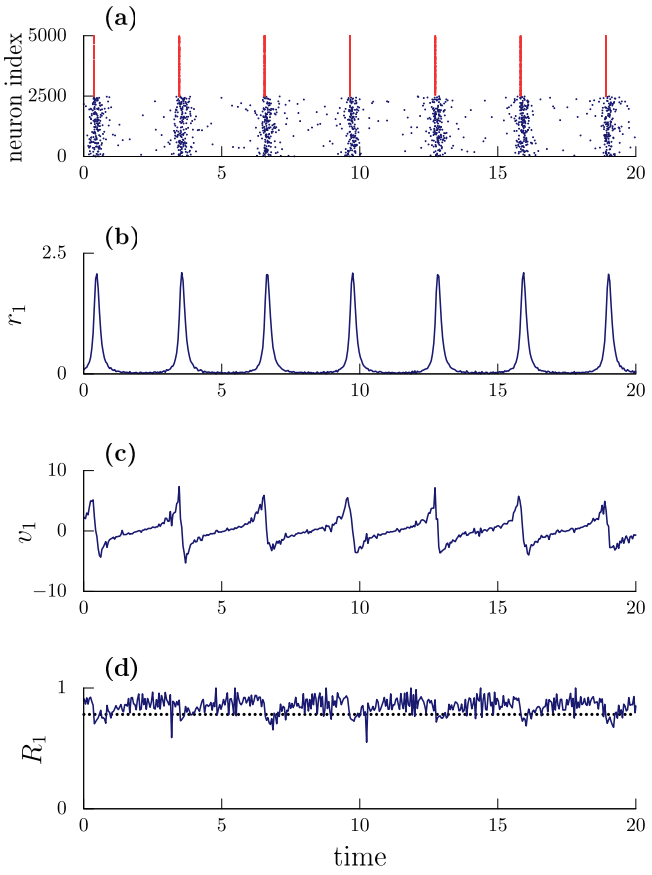

FIG. 5. Periodic chimera state in a two-population network of $N = 5000$ identical inhibitory QIF neurons ($n = 2500$ neurons in each population). (a) Raster plot of 500 randomly chosen neurons. Neurons in population 1 (blue) are partially synchronized, and neurons on population 2 are in-phase synchronized (red). (b) Time series of the mean firing rate r_1 of population 1, computed averaging the firing rate at each time step in time windows of $\delta t = 0.05$. (c) Time series of the mean membrane potential v_1 of population 1. (d) Time series of the Kuramoto order parameter of population 1, R_1, obtained from the mean-field quantities r_1, v_1 using the conformal map [Eq. (33)] (blue lines) and from direct integration of Eq. (32) (black dots). Parameters as in Fig. 4(d) [see also + symbol in Fig. 3(b)]: $J_c/J_s = 0.75$, $g_c/g_s = 0.5$, $\rho_s = -40/\pi$, and $g_s = 0.1$. Numerical simulations performed using the Euler scheme with time step: $dt = 10^{-4}$ and symmetric resetting: $V_p = -V_r = 1000$.

2. Chimeras for strong coupling

The derivation of Eq. (27) from the QIF network [Eq. (26)] has been made under the assumption of weak coupling. Yet, are chimera states in QIF networks robust against stronger levels of coupling?

To investigate this issue, we used the conformal map [Eq. (33)] to express the boundary of the basin of attraction of Fig. 4(a) in terms of (r_1, v_1). This transformed boundary is represented as a dashed line in Figs. 4(b)–4(d). Then, we performed three sets of numerical simulations of the QIF network for increasing values of g_s while keeping the ratios g_c/g_s, J_c/J_s, and ρ_s constant—note that this implies increasing all the other coupling parameters.

For very small values of g_s, we expect the averaging approximation to hold and hence the stability boundary of chimera states in the QIF model. The green-dotted region in Fig. 4(b) corresponds to the stability boundary of the steady chimera state in the QIF network for $g_s = 0.025$. The boundary approximately agrees with that of the KM (dashed line), although the region is slightly smaller in the QIF model. Notably, further increases in coupling strength—see Figs. 4(c) and 4(d)—lead to a gradual reduction of the chimera's basin of attraction.

To further investigate the reduction of the stability boundary of chimeras in the QIF model, in Figs. 4(f)–4(h), we computed the basins of attraction of chimera states in a different parameter regime—corresponding to the + symbol in Fig. 3(a). Here, $|\rho_s|$ is

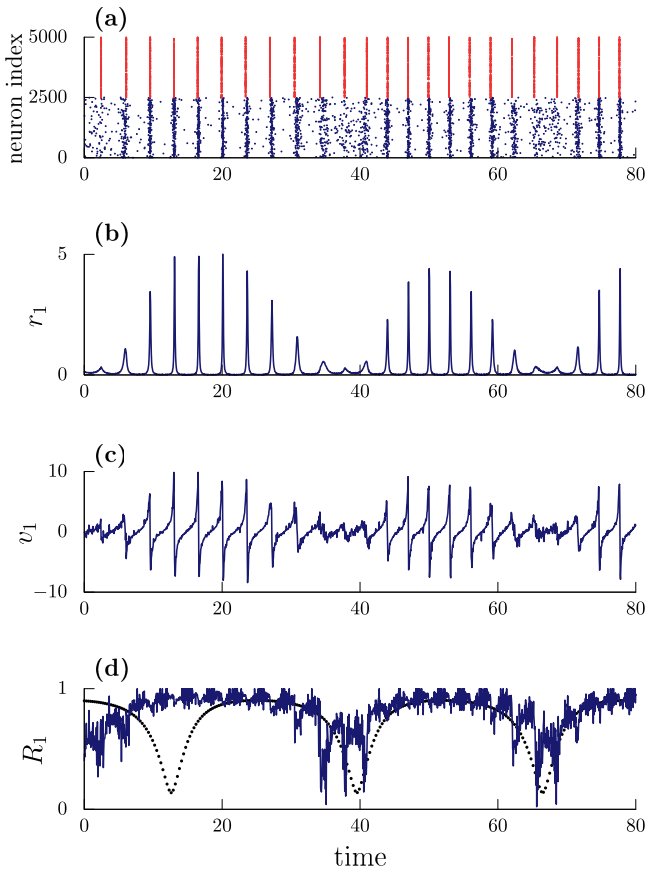

FIG. 6. Quasiperiodic chimera state in a two-population network of $N = 5\,000$ identical inhibitory QIF neurons. The description of the panels and parameters is as in Fig. 5 except $J_c/J_s = 0.5$ [see also the $\times$ symbol in Fig. 3(b)].

three times larger than in the previous case, and hence, chemical couplings are three times stronger than in Figs. 4(b)–4(d). Correspondingly, the reduction of the basin of attraction of chimera states in Figs. 4(f)–4(h) is more pronounced than in Figs. 4(b)–4(d). In fact, in Fig. 4(h), we find the complete disappearance of the region of stable chimera states in the QIF network. This suggests that chimera states in QIF networks are only observable for weak coupling.

VI. CONCLUSIONS

In this paper, we have applied a perturbative approach to simplify a weakly heterogeneous population of QIF neurons, with weak all-to-all chemical and electrical coupling [Eq. (1)]. This approach leads to a classical variant of the Kuramoto model [Eq. (19)],[28,29] whose coupling parameters satisfy a simple geometric relation with those of the QIF model (Fig. 1).[83]

The approximation of the QIF network by Eq. (19) allows one to use the framework of the KM to investigate the role of chemical and electrical synapses in setting up synchronization. For example, we find that in the absence of electrical coupling, the phase lag parameter of the KM is $\alpha = \pm\pi/2$, which prohibits synchronization; see also Ref. 45. Moreover, for Lorentzian distributions of currents, the synchronization threshold depends only on electrical coupling, Eq. (24), whereas the oscillation frequency [Eq. (25)] is determined by the ratio of chemical to electrical coupling. These results are in consonance with the exact description provided by so-called neural mass (or firing rate) models for networks of QIF neurons.[37,38]

The framework of the KM allows for uncovering and investigating dynamical states that are not reachable using neural mass models for QIF neurons.[37–39,48] Here, we analyzed the case of chimera states in two-population networks of identical QIF neurons.[40,41] Despite the large number of studies devoted to investigate chimera states in spiking neuron networks—see, e.g., Refs. 60–69—the relation between such states and the original chimera states uncovered in the KM[40,41,58] is lacking.[70,72] We showed that chimera states in QIF networks emerge in the presence of both chemical and electrical couplings but only if chemical coupling is much stronger than electrical coupling. However, our numerical results suggest that chimeras in QIF networks are not robust against stronger levels of coupling.

Finally, we introduced a framework for the analysis of QIF networks that can be readily applied to a variety of extensions of Eq. (1). In particular, the derivation of Eq. (19) does not impose constraints on the structure of the network or the shape of the distribution of heterogeneities. Given that the network structure[28,53] and heterogeneities[84–89] greatly affect the dynamics of the KM, it may be interesting to investigate how this translates to QIF networks.

ACKNOWLEDGMENTS

The authors thank Diego Pazó for helpful discussions. P.C. acknowledges financial support from the European Union's Horizon 2020 research and innovation program under Grant Agreement No. 101017716 (Neurotwin). E.M. acknowledges support by the Agencia Estatal de Investigación under Project No. PID2019-109918GB-I00.

AUTHOR DECLARATIONS

Conflict of Interest

The authors have no conflicts to disclose.

DATA AVAILABILITY

Data sharing is not applicable to this article as no new data were created or analyzed in this study.

REFERENCES

[1] Y. Kuramoto, "Self-entrainment of a population of coupled non-linear oscillators," in *International Symposium on Mathematical Problems in Theoretical Physics*, Lecture Notes in Physics, Vol. 39, edited by H. Araki (Springer, Berlin, 1975), pp. 420–422.
[2] Y. Kuramoto, *Chemical Oscillations, Waves, and Turbulence* (Springer-Verlag, Berlin, 1984).
[3] K. Glomb, J. Cabral, A. Cattani, A. Mazzoni, A. Raj, and B. Franceschiello, "Computational models in electroencephalography," Brain Topogr. **2021**, 1–20.

[4]C. W. Lynn and D. S. Bassett, "The physics of brain network structure, function and control," Nat. Rev. Phys. **1**, 318–332 (2019).
[5]M. Breakspear, S. Heitmann, and A. Daffertshofer, "Generative models of cortical oscillations: Neurobiological implications of the Kuramoto model," Front. Hum. Neurosci. **4**, 190 (2010).
[6]J. Cabral, E. Hugues, O. Sporns, and G. Deco, "Role of local network oscillations in resting-state functional connectivity," NeuroImage **57**, 130–139 (2011).
[7]P. Villegas, P. Moretti, and M. A. Muñoz, "Frustrated hierarchical synchronization and emergent complexity in the human connectome network," Sci. Rep. **4**, 5990 (2014).
[8]A. Ponce-Alvarez, G. Deco, P. Hagmann, G. L. Romani, D. Mantini, and M. Corbetta, "Resting-state temporal synchronization networks emerge from connectivity topology and heterogeneity," PLoS Comput. Biol. **11**, e1004100 (2015).
[9]P. Sanz-Leon, S. A. Knock, A. Spiegler, and V. K. Jirsa, "Mathematical framework for large-scale brain network modeling in the virtual brain," NeuroImage **111**, 385–430 (2015).
[10]R. Schmidt, K. J. R. LaFleur, M. A. de Reus, L. H. van den Berg, and M. P. van den Heuvel, "Kuramoto model simulation of neural hubs and dynamic synchrony in the human cerebral connectome," BMC Neurosci. **16**, 54 (2015).
[11]S. Petkoski, A. Spiegler, T. Proix, P. Aram, J.-J. Temprado, and V. K. Jirsa, "Heterogeneity of time delays determines synchronization of coupled oscillators," Phys. Rev. E **94**, 012209 (2016).
[12]R. G. Andrzejak, C. Rummel, F. Mormann, and K. Schindler, "All together now: Analogies between chimera state collapses and epileptic seizures," Sci. Rep. **6**, 23000 (2016).
[13]S. Petkoski, J. M. Palva, and V. K. Jirsa, "Phase-lags in large scale brain synchronization: Methodological considerations and in-silico analysis," PLoS Comput. Biol. **14**, 1006160 (2018).
[14]J. A. Roberts, L. L. Gollo, R. G. Abeysuriya, G. Roberts, P. B. Mitchell, M. W. Woolrich, and M. Breakspear, "Metastable brain waves," Nat. Commun. **10**, 1 (2019).
[15]H. Choi and S. Mihalas, "Synchronization dependent on spatial structures of a mesoscopic whole-brain network," PLoS Comput. Biol. **15**, e1006978 (2019).
[16]A. Ziaeemehr, M. Zarei, A. Valizadeh, and C. R. Mirasso, "Frequency-dependent organization of the brain's functional network through delayed-interactions," Neural Netw. **132**, 155–165 (2020).
[17]R. Noori, D. Park, J. D. Griffiths, S. Bells, P. W. Frankland, D. Mabbott, and J. Lefebvre, "Activity-dependent myelination: A glial mechanism of oscillatory self-organization in large-scale brain networks," Proc. Natl. Acad. Sci. U.S.A. **117**, 13227–13237 (2020).
[18]K. Jung, S. B. Eickhoff, and O. V. Popovych, "Tractography density affects whole-brain structural architecture and resting-state dynamical modeling," NeuroImage **237**, 118176 (2021).
[19]P. K. Tewarie, B. Prasse, J. M. Meier, Á. Byrne, M. D. Domenico, C. J. K. Stam, M. J. Brookes, A. Hillebrand, A. Daffertshofer, S. Coombes, and P. V. Mieghem, "Interlayer connectivity reconstruction for multilayer brain networks using phase oscillator models," New J. Phys. **23**, 063065 (2021).
[20]G. Ódor, J. Kelling, and G. Deco, "The effect of noise on the synchronization dynamics of the Kuramoto model on a large human connectome graph," Neurocomputing **461**, 696–704 (2021).
[21]J. C. Pang, L. L. Gollo, and J. A. Roberts, "Stochastic synchronization of dynamics on the human connectome," NeuroImage **229**, 117738 (2021).
[22]G. Weerasinghe, B. Duchet, C. Bick, and R. Bogacz, "Optimal closed-loop deep brain stimulation using multiple independently controlled contacts," PLoS Comput. Biol. **17**, e1009281 (2021).
[23]X.-J. Wang, "Neurophysiological and computational principles of cortical rhythms in cognition," Physiol. Rev. **90**, 1195–1268 (2010).
[24]C. Börgers, *An Introduction to Modeling Neuronal Dynamics* (Springer, 2017), Vol. 66.
[25]B. Ermentrout, "Type I membranes, phase resetting curves, and synchrony," Neural Comput. **8**, 979–1001 (1996).
[26]B. Ermentrout and N. Kopell, "Parabolic bursting in an excitable system coupled with a slow oscillation," SIAM J. Appl. Math. **46**, 233–253 (1986).
[27]E. M. Izhikevich, *Dynamical Systems in Neuroscience* (The MIT Press, Cambridge, MA, 2007).
[28]H. Sakaguchi, S. Shinomoto, and Y. Kuramoto, "Mutual entrainment in oscillator lattices with nonvariational type interaction," Prog. Theor. Phys. **79**, 1069–1079 (1988).
[29]H. Sakaguchi and Y. Kuramoto, "A soluble active rotator model showing phase transitions via mutual entrainment," Prog. Theor. Phys. **76**, 576–581 (1986).
[30]A. S. Pikovsky, M. G. Rosenblum, and J. Kurths, *Synchronization, a Universal Concept in Nonlinear Sciences* (Cambridge University Press, Cambridge, 2001).
[31]S. H. Strogatz, "From Kuramoto to Crawford: Exploring the onset of synchronization in populations of coupled oscillators," Physica D **143**, 1–20 (2000).
[32]A. Pikovsky and M. Rosenblum, "Dynamics of globally coupled oscillators: Progress and perspectives," Chaos **25**, 097616 (2015).
[33]X.-J. Wang and G. Buzsáki, "Gamma oscillation by synaptic inhibition in a hippocampal interneuronal network model," J. Neurosci. **16**, 6402–6413 (1996).
[34]H. R. Wilson and J. D. Cowan, "Excitatory and inhibitory interactions in localized populations of model neurons," Biophys. J. **12**, 1–24 (1972).
[35]J. I. Nagy, A. E. Pereda, and J. E. Rash, "Electrical synapses in mammalian CNS: Past eras, present focus and future directions," Biochim. Biophys. Acta Biomembr. **1860**, 102–123 (2018).
[36]G. Deco, G. Tononi, M. Boly, and M. L. Kringelbach, "Rethinking segregation and integration: Contributions of whole-brain modelling," Nat. Rev. Neurosci. **16**, 430–439 (2015).
[37]B. Pietras, F. Devalle, A. Roxin, A. Daffertshofer, and E. Montbrió, "Exact firing rate model reveals the differential effects of chemical versus electrical synapses in spiking networks," Phys. Rev. E **100**, 042412 (2019).
[38]E. Montbrió and D. Pazó, "Exact mean-field theory explains the dual role of electrical synapses in collective synchronization," Phys. Rev. Lett. **125**, 248101 (2020).
[39]E. Montbrió, D. Pazó, and A. Roxin, "Macroscopic description for networks of spiking neurons," Phys. Rev. X **5**, 021028 (2015).
[40]E. Montbrió, J. Kurths, and B. Blasius, "Synchronization of two interacting populations of oscillators," Phys. Rev. E **70**, 056125 (2004).
[41]D. M. Abrams, R. Mirollo, S. H. Strogatz, and D. A. Wiley, Phys. Rev. Lett. **101**, 084103 (2008).
[42]C. R. Laing, "Chimera states in heterogeneous networks," Chaos **19**, 013113 (2009).
[43]E. A. Martens, C. Bick, and M. J. Panaggio, "Chimera states in two populations with heterogeneous phase-lag," Chaos **26**, 094819 (2016).
[44]D. Pazó and E. Montbrió, "Low-dimensional dynamics of populations of pulse-coupled oscillators," Phys. Rev. X **4**, 011009 (2014).
[45]E. Montbrió and D. Pazó, "Kuramoto model for excitation-inhibition-based oscillations," Phys. Rev. Lett. **120**, 244101 (2018).
[46]More recently, a similar derivation has been obtained for populations of heterogeneous Winfree oscillators with sinusoidal infinitesimal phase resetting curves (iPRCs).[44] When the oscillators have the iPRC of the QIF neuron, the population of Winfree oscillators can be well approximated to a population of QIF neurons with (weak) chemical synapses.[45]
[47]N. Kopell and B. Ermentrout, "Chemical and electrical synapses perform complementary roles in the synchronization of interneuronal networks," Proc. Natl. Acad. Sci. U.S.A. **101**, 15482–15487 (2004).
[48]C. R. Laing, "Exact neural fields incorporating gap junctions," SIAM J. Appl. Dyn. Syst. **14**, 1899–1929 (2015).
[49]F. C. Hoppensteadt and E. M. Izhikevich, *Weakly Connected Neural Networks* (Springer-Verlag, New York, 1997).
[50]B. Pietras and A. Daffertshofer, "Network dynamics of coupled oscillators and phase reduction techniques," Phys. Rep. **819**, 1–105 (2019).
[51]A. T. Winfree, "Biological rhythms and the behavior of populations of coupled oscillators," J. Theor. Biol. **16**, 15–42 (1967).
[52]For $g = 0$, the natural frequencies in Refs. 44 and 45 differ from Eq. (18). The reason for this discrepancy is that Refs. 44 and 45 consider the Winfree model with distributed natural frequencies Ω_i, while here, we study the QIF model with distributed currents η_i.
[53]B. Blasius and R. Tönjes, "Quasiregular concentric waves in heterogeneous lattices of coupled oscillators," Phys. Rev. Lett. **95**, 084101 (2005).
[54]D. Hansel, G. Mato, and C. Meunier, "Synchrony in excitatory neural networks," Neural Comput. **7**, 307–337 (1995).

[55]F. Devalle, A. Roxin, and E. Montbrió, "Firing rate equations require a spike synchrony mechanism to correctly describe fast oscillations in inhibitory networks," PLoS Comput. Biol. **13**, e1005881 (2017).
[56]E. Ott and T. M. Antonsen, "Low dimensional behavior of large systems of globally coupled oscillators," Chaos **18**, 037113 (2008).
[57]E. Montbrió and D. Pazó, "Shear diversity prevents collective synchronization," Phys. Rev. Lett. **106**, 254101 (2011).
[58]Y. Kuramoto and D. Battogtokh, "Coexistence of coherence and incoherence in nonlocally coupled phase oscillators," Nonlinear Phenom. Complex Syst. **5**, 380 (2002).
[59]H. Sakaguchi, "Instability of synchronized motion in nonlocally coupled neural oscillators," Phys. Rev. E **73**, 031907 (2006).
[60]S. Olmi, A. Politi, and A. Torcini, "Collective chaos in pulse-coupled neural networks," Europhys. Lett. **92**, 60007 (2010).
[61]I. Omelchenko, O. E. Omel'chenko, P. Hövel, and E. Schöll, "When nonlocal coupling between oscillators becomes stronger: Patched synchrony or multichimera states," Phys. Rev. Lett. **110**, 224101 (2013).
[62]A. Vüllings, J. Hizanidis, I. Omelchenko, and P. Hövel, "Clustered chimera states in systems of type-I excitability," New J. Phys. **16**, 123039 (2014).
[63]J. Hizanidis, V. G. Kanas, A. Bezerianos, and T. Bountis, "Chimera states in networks of nonlocally coupled Hindmarsh–Rose neuron models," Int. J. Bifurcation Chaos **24**, 1450030 (2014).
[64]M. J. Panaggio and D. M. Abrams, "Chimera states: Coexistence of coherence and incoherence in networks of coupled oscillators," Nonlinearity **28**, R67 (2015).
[65]S. Majhi, B. K. Bera, D. Ghosh, and M. Perc, "Chimera states in neuronal networks: A review," Phys. Life Rev. **28**, 100–121 (2019).
[66]C. R. Laing, "Dynamics and stability of chimera states in two coupled populations of oscillators," Phys. Rev. E **100**, 042211 (2019).
[67]J. Hizanidis, N. E. Kouvaris, G. Zamora-López, A. Díaz-Guilera, and C. G. Antonopoulos, "Chimera-like states in modular neural networks," Sci. Rep. **6**, 19845 (2016).
[68]M. Gerster, R. Berner, J. Sawicki, A. Zakharova, A. Škoch, J. Hlinka, K. Lehnertz, and E. Schöll, "FitzHugh–Nagumo oscillators on complex networks mimic epileptic-seizure-related synchronization phenomena," Chaos **30**, 123130 (2020).
[69]A. Lucchetti, M. H. Jensen, and M. L. Heltberg, "Emergence of chimera states in a neuronal model of delayed oscillators," Phys. Rev. Res. **3**, 033041 (2021).
[70]C. Bick, M. Goodfellow, C. R. Laing, and E. A. Martens, "Understanding the dynamics of biological and neural oscillator networks through exact mean-field reductions: A review," J. Math. Neurosci. **10**, 9 (2020).
[71]O. E. Omel'chenko, "The mathematics behind chimera states," Nonlinearity **31**, R121 (2018).
[72]S. W. Haugland, "The changing notion of chimera states, a critical review," J. Phys. Complex. **2**, 032001 (2021).
[73]A. Byrne, J. Ross, R. Nicks, and S. Coombes, "Mean-field models for EEG/MEG: From oscillations to waves," Brain Topogr. **2021**, 1–18.
[74]NMMs for QIF neurons are derived after adopting the thermodynamic limit, $N \to \infty$, and under the assumption $V_r \to -\infty$ and $V_p \to \infty$; see Refs. 38 and 39. If neurons are fully synchronized, $[V_i(t) = V_j(t), \forall i, j]$, the population of QIF neurons behaves as a single neuron. Therefore, in QIF-NMM, the mean voltage [Eq. (3)] diverges when all neurons fire a spike—in Refs. 48 and 90, the mean-field variable v is approximated to avoid this divergence; see also Ref. 37.
[75]C.-U. Choe, J.-S. Ri, and R.-S. Kim, "Incoherent chimera and glassy states in coupled oscillators with frustrated interactions," Phys. Rev. E **94**, 032205 (2016).
[76]A. Pikovsky and M. Rosenblum, "Partially integrable dynamics of hierarchical populations of coupled oscillators," Phys. Rev. Lett. **101**, 264103 (2008).
[77]S. Watanabe and S. H. Strogatz, "Constant of motion for superconducting Josephson arrays," Physica D **74**, 197–253 (1994).
[78]Y. Kawamura, H. Nakao, K. Arai, H. Kori, and Y. Kuramoto, "Phase synchronization between collective rhythms of globally coupled oscillator groups: Noiseless nonidentical case," Chaos **20**, 043110 (2010).
[79]E. J. Doedel, "AUTO: A program for the automatic bifurcation analysis of autonomous systems," Congr. Numer **30** (265–284), 25–93 (1981).
[80]Figures 4(b)–4(f) in Ref. 43 show a bifurcation scenario with a transcritical bifurcation that is not observed in Fig. 3. This bifurcation occurs for $\alpha_s > \pi/2$, and these values of the phase lag parameter are unreachable in the QIF model, where $\alpha_s \in (-\pi/2, 0)$ for inhibitory coupling and $\alpha_s \in (0, \pi/2)$ for excitatory coupling; see Eq. (29).
[81]For $n \to \infty$, this corresponds to a Lorentzian distribution of voltages $\rho(V) = \pi\tau r/[(V-v)^2 + (\pi\tau r)^2]$, see Ref. 39, and to uniformly distributed constants of motion in the Watanabe–Strogatz theory.[70,76,91]
[82]We cannot discount that the collective dynamics of the QIF [Eq. (26)] is chaotic, as it also occurs in coupled populations of Winfree oscillators.[44]
[83]A similar approach has been applied to the leaky integrate-and-fire model. In this case, the approximated phase model is not the KM, but it contains higher harmonics in the coupling function.[92]
[84]D. Pazó, "Thermodynamic limit of the first order phase transition in the Kuramoto model," Phys. Rev. E **72**, 046211 (2005).
[85]L. F. Lafuerza, P. Colet, and R. Toral, "Nonuniversal results induced by diversity distribution in coupled excitable systems," Phys. Rev. Lett. **105**, 084101 (2010).
[86]O. E. Omel'chenko and M. Wolfrum, "Nonuniversal transitions to synchrony in the Sakaguchi-Kuramoto model," Phys. Rev. Lett. **109**, 164101 (2012).
[87]E. A. Martens, E. Barreto, S. H. Strogatz, E. Ott, P. So, and T. M. Antonsen, "Exact results for the Kuramoto model with a bimodal frequency distribution," Phys. Rev. E **79**, 026204 (2009).
[88]D. Pazó and E. Montbrió, "Existence of hysteresis in the Kuramoto model with bimodal frequency distributions," Phys. Rev. E **80**, 046215 (2009).
[89]B. Pietras, N. Deschle, and A. Daffertshofer, "First-order phase transitions in the Kuramoto model with compact bimodal frequency distributions," Phys. Rev. E **98**, 062219 (2018).
[90]B. Ermentrout, "Gap junctions destroy persistent states in excitatory networks," Phys. Rev. E **74**, 031918 (2006).
[91]C. R. Laing, "The dynamics of networks of identical theta neurons," J. Math. Neurosci. **8**, 4 (2018).
[92]A. Politi and M. Rosenblum, "Equivalence of phase-oscillator and equivalence of phase-oscillator and integrate-and-fire models," Phys. Rev. E **91**, 042916 (2015).